

3-D quantitative analysis of brain SPECT images

Sven Loncaric , Ivan Ceškovic, Ratimir Petrovic*, Srecko Loncaric*
Faculty of Electrical Engineering and Computing, University of Zagreb
Unska 3, 10000 Zagreb, Croatia
sven.loncaric@fer.hr, iceskov@fly.srk.fer.hr

*Dept. of Nuclear Medicine and Radiation Protection, University Hospital Zagreb, KBC – Rebro,
Kišpaticeva 12, 10000 Zagreb, Croatia

ABSTRACT

The main purpose of this work is to develop a computer-based technique for quantitative analysis of 3-D brain images obtained by single photon emission computed tomography (SPECT). In particular, the volume and location of ischemic lesion and penumbra is important for early diagnosis and treatment of infarcted regions of the brain. SPECT imaging is typically used as diagnostic tool to assess the size and location of the ischemic lesion. The segmentation method presented in this paper utilizes a 3-D deformable model in order to determine size and location of the regions of interest. The evolution of the model is computed using a level-set implementation of the algorithm. In addition to 3-D deformable model the method utilizes edge detection and region growing for realization of a pre-processing. Initial experimental results have shown that the method is useful for SPECT image analysis.

Keywords: deformable model, level-set algorithm, image segmentation, SPECT

1. INTRODUCTION

The volume and location of certain regions of interest such as ischemic lesion is important for early diagnosis and treatment of various cerebrovascular accidents and diseases. Penumbra is a region near the border of ischemic lesion which consists of partially damaged nerve cells. The size and location of penumbra in ischemic lesion is important because by appropriate therapy it is possible to reduce the damage and recover nerve cells in penumbra. SPECT imaging is typically used as diagnostic tool to assess the size and location of the ischemic lesion.

In this paper we describe a method for segmentation of brain SPECT images based on deformable models. The characteristics of images from an SPECT camera played a central role in choosing a segmentation method. Due to an extremely low resolution and high amount of noise, we had to use a robust segmentation algorithm, so we utilize a level-set algorithm for implementation of the deformable models method. Once the 3D model of desired region (lesion, tumor) is available, it is relatively easy to perform quantitative analysis such as calculating a volume. This information can be utilized in diagnostic and treatment of various cerebrovascular accidents and diseases.

2. LEVEL SET BASED SEGMENTATION METHOD

Deformable models were introduced by Terzopoulos *et al.* in the mid-1980s [1]. Terzopoulos introduced the theory of continuous deformable models based on deformation energies in the form of generalized splines. Kass *et al.* [3]. later introduced the deformable model that attracted the most attention – ‘snakes’. Snakes represent a special case of the general multidimensional deformable model theory.

In this work, we use a level set approach to deformable models introduced by J.A. Sethian [5]. Level set approach has numerous advantages over classical active contour approach. The major advantage is the ability to change topology and segment complex structures. The level set approach to object detection hides the active contour as the zero level set of a higher dimensional function. While this function stays smooth, it's zero level set can take any possible shape. Another advantage of the level set method over the classical active contour approach is that the level set can be applied without any *a priori* assumption about the object's topology. In this section we provide a description of the 2D level set approach.

As we mentioned above, in the level set approach a 2D curve γ is represented by a 3D surface Ψ . Let $\gamma(t=0)$ be a smooth, closed initial curve in the Euclidian plane \mathfrak{R}^2 , and let $\gamma(t)$ be a family of curves generated by moving $\gamma(t=0)$ along its normal vector field with speed $F(K)$ where K represents the curvature. The propagating front ($\gamma(t)$) is embedded as the zero level set ($\Psi=0$) of the higher dimensional function Ψ . $\Psi(x, t=0)$, where $\mathbf{x} \in \mathfrak{R}^2$ are points in the image space, is defined by:

$$\Psi(x, t = 0) = \pm d \quad (1)$$

where d is the distance from the point \mathbf{x} to $\gamma(t=0)$, and the sign depends on the position of the point \mathbf{x} considering the initial surface $\gamma(t=0)$. If \mathbf{x} is outside (inside) the initial surface the sign is plus (minus). See Figure 1.

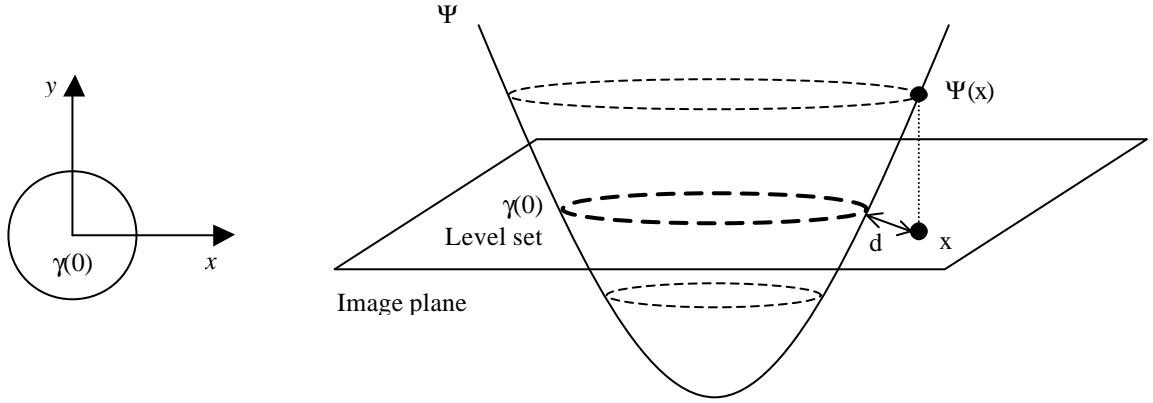


Figure 1. Level set illustration

The next step is to produce an equation for the evolving function $\Psi(x,t)$ which contains the embedded $\gamma(t)$ as the zero level set. Let $\mathbf{x}(t)$, $t \in [0, \infty)$ be the path of a point on the propagating front. Since $\Psi(\mathbf{x}(t), t) = 0$ we have the evolution equation for Ψ :

$$\frac{\partial \Psi(x, t)}{\partial t} + F|\nabla \Psi| = 0 \quad (2)$$

To obtain numerical solution of Equation 2, it is necessary to perform discretization in both space and time domains. Let Ψ_{ij}^n be the approximation to the solution $\Psi(ih, jh, n\Delta t)$, where h is the spacing on a uniform mesh and Δt is the time step. That gives us the final iteration expression:

$$\Psi_{ij}^{n+1} = \Psi_{ij}^n - \Delta t F |\nabla_{ij} \Psi_{ij}^n| \quad (3)$$

The speed term F depends on the curvature K . We can separate $F(K)$ into a constant advection term F_0 and the remainder $F_1(K)$.

$$F(K) = F_0 + F_1(K) \quad (4)$$

Term F_0 represents a uniform direction speed of the front and is independent of the moving front's geometry. The front uniformly expands (or contracts, depending on its sign) with speed F_0 and it is analogous to the inflation force in the classic

active contour approach. Diffusion term $F_f(K)$ depends on the geometry of the front, such as its local curvature. It smoothes out the high curvature regions and is similar to the internal deformation forces in the classical snake models.

The curvature is obtained from the divergence of the gradient of the unit normal vector to front:

$$K = \nabla \cdot \frac{\nabla \Psi}{|\nabla \Psi|} = -\frac{\Psi_{xx} \Psi_y^2 - 2\Psi_x \Psi_y \Psi_{xy} + \Psi_{yy} \Psi_x^2}{(\Psi_x^2 + \Psi_y^2)^{3/2}} \quad (5)$$

Image information is integrated into the speed term of Equation 4. In order to segment images the image information implemented into Equation 4. has to stop the propagating front near desired objects boundary. This is done by multiplying the speed function F with a quantity k . The term k is defined as:

$$k(x, y) = e^{-|\nabla G_\sigma \cdot I(x, y)|} \quad (6)$$

where $G_\sigma \cdot I(x, y)$ denotes the image convolved with Gaussian smoothing filter whose characteristic width is σ .

Sethian *et al* [X] proposed several extensions of the speed function. We use the narrow-band extension with reinitialization where the front is moved by updating the level set function at a small set of points in the neighborhood of the zero set called the narrow band, instead of updating it at all the points on the grid (Figure 2.). The narrow band is bounded on either side by two curves that are a distance δ apart. The zero set that lies inside moves until it collides with one of the boundaries, at which point we must rebuild an appropriate narrow band.

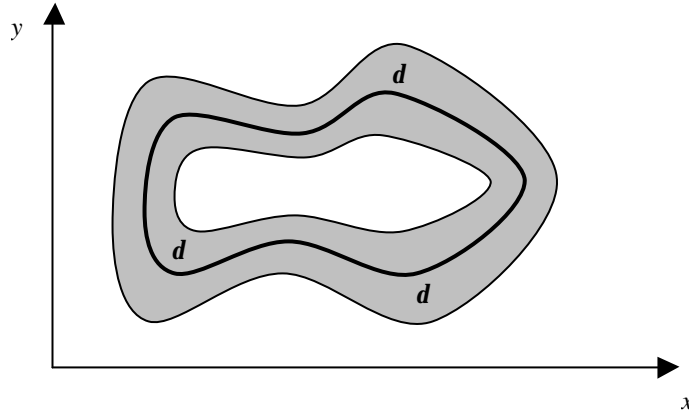


Figure 2. A narrow band of width δ

3. BRAIN IMAGE SEGMENTATION

We apply the level set method described above to the problem of segmentation regions of interest in the brain SPECT images. The input is the 3D SPECT image of human brain.

In order to use the level set algorithm the initial contour has to be defined. We use a circle for its simplicity. The circle center and radius have to be defined manually by the user so that it lies inside the region of interest. The algorithm shown in Table 1. evolves the initial curve γ_1 through its corresponding higher dimensional surface Ψ_1 until it stops changing.

```

initialize  $\Psi$ ;
current contour = Initial contour;
compute initial narrow band;
while (current contour != previous contour) {

```

```

for (i=1 to N) do
    iterate Equation 4;
previous contour = current contour;
trace current contour;
reinitialise  $\Psi$ ;
recalculate narrow band;
}

```

Table 1. Level set algorithm

The output of the algorithm is the final surface representing the boundary of the region of interest.

Due to the input images low resolution, high amount of noise and fuzziness we had some problems in calculating the gradient of the image with the simple Gaussian filter. We used a zero-crossing image of the original image convolved with a Laplacian-of-Gaussian filter with characteristic width σ . Thus we modified Equation 6:

$$k(x, y) = e^{-|\nabla^2 G_\sigma \cdot I(x, y)|} \quad (7)$$

The region of interest may have a neighboring region that has accumulated a similar amount of radioactive isotopes and has the same intensity in the image thus making it impossible to determine the border between them. Level-set algorithm can successfully deal with small contact areas by increasing the curvature dependant speed term $F_I(K)$, but can not stop propagation of the zero level-set outside the region of interest if the contact area is very large. We tried to overcome this problem by adding additional stopping criteria gained by tresholding the input image and computing the gradient. The gradient of tresholded image is then added as an additional stopping criteria. This method requires high amount of user intervention since the treshold has to be defined so that most of its edges overlapped the edges gained by the zero-crossing. It also raised numerous other problems without completely solving the problem of contacting regions. Another way of user assistance is to place a few control points along the problematic boundaries as suggested by S. Loncaric *et al.* [6], but that way of user intervention would require the user to go through every slice in the image. The stopping criteria is extended to include these control points: the algorithm stops if all or most of the control points are inside the evolving front.

The algorithm has been implemented in C++ programming language and an appropriate user interface (Figure 3.) was developed using Borland Builder package.

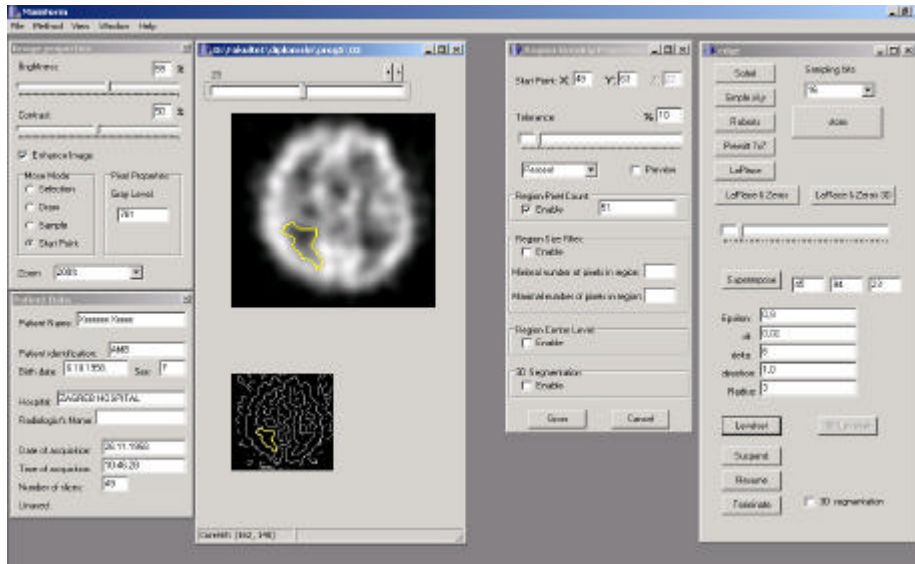


Figure 3. User interface

4. RESULTS

The algorithm has been tested using SPECT brain images of real patients. Input image consisted of 41 slices of dimensions 128×128 . Values of numerical constants: $F_0=1$, $\epsilon=0.8$ so that smaller breaks in the gradient image were handled. Width of the narrow band $\delta=6$.

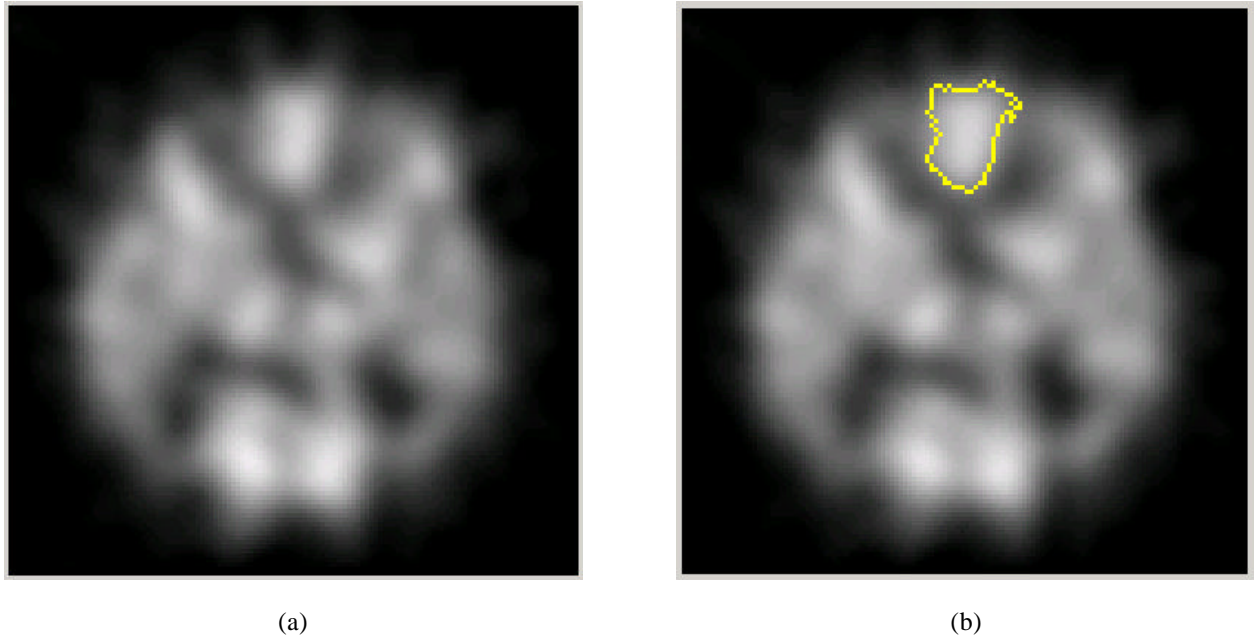


Figure 4. (a) Input slice, (b) Result: segmented frontal lobe

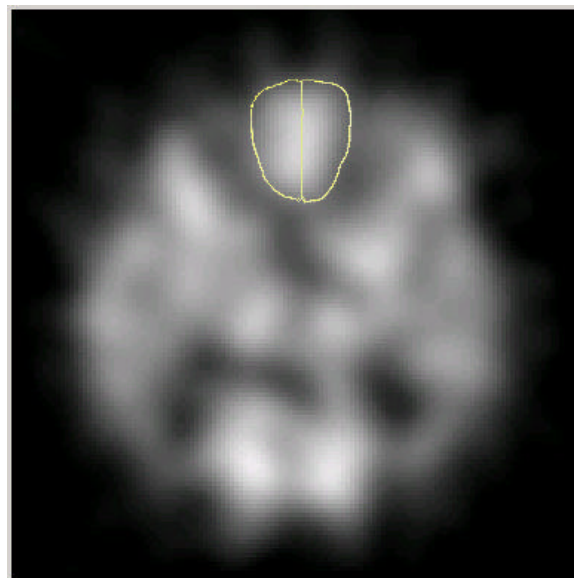


Figure 5. Manually segmented input slice

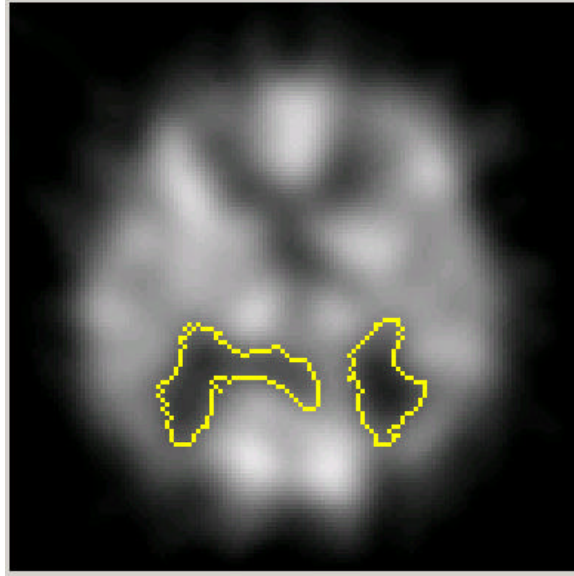


Figure 6. Segmented ventricles. The problem with bordering regions of the same intensity is visible with the left ventricle.

Figures 4. and 6. show the result of segmentation using the proposed algorithm, and Figure 5. shows manual segmentation of the same slice. In Figure 4a. we have the input image, and in the Figure 4b. segmented frontal region using the proposed algorithm. The main purpose in developing this work was to segment regions without activity, such as lesions or tumors. In Figure 6. we used the algorithm to segment region without activity (brain ventricles) on the same input image as in the first example. It is clearly visible that the left ventricle was not segmented correctly due to its proximity to another region without activity (region of low intensity). The problem was solved by adding additional stopping criteria gained by thresholding. The result is shown in the Figure 7.

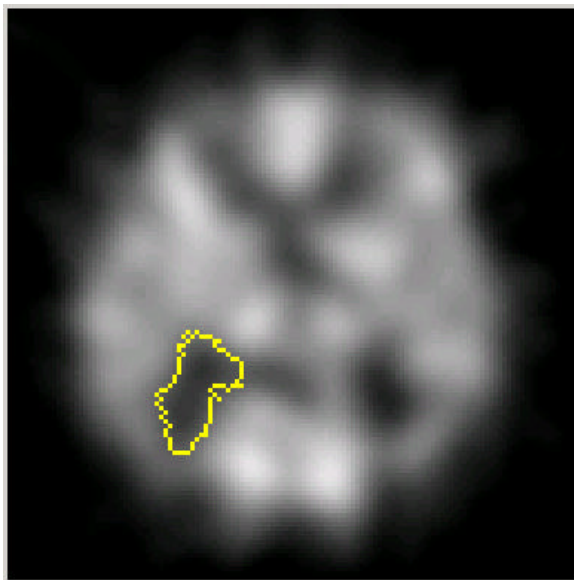


Figure 7. Left ventricle segmented with an additional stopping criteria

Segmentation was performed on each slice containing the region (slices containing the region were selected by the region growing method as a preprocessing step) and the number of voxels inside the region were counted.

5. CONCLUSION

The main purpose of this work was to propose a method for quantitative analysis of brain SPECT images. We showed that the level set method can be successfully used to segment regions of interest as brain structures or regions without activity (dark regions). Results are encouraging for further research in this direction. Different methods for gradient computation will be included in future work. Also the stopping criteria will have to be modified if bordering regions are to be separated with lesser amount of manual user assistance. We are also developing a 3D visualization of input data and segmented regions as an additional data representation method.

1. D. Terzopoulos, "On matching Deformable Models to Images", Topical Meeting on Machine Vision, Vol. 12, 1987, pp. 160-167
2. T. McInerney and D. Terzopoulos, "Deformable Models in Medical Image Analysis: A Survey", Medical Image Analysis, Vol. 1, No. 2, 1996, pp. 91-108
3. M. Kass, A. Witkin, and D. Terzopoulos, "Snakes: Active Contour Models", International Journal of Computer Vision, Vol. 1, pp.32-33
4. S. Loncaric, D. Kovacevic, and E. Sorantin, "Semi-automatic active contour approach to segmentation of computed tomography volumes", Proceedings of SPIE Medical Imaging, 2000, Vol. 3979
5. R. Malladi, J.A. Sethian, and B.C. Vemuri, "Shape modeling with front propagation: A Level Set Approach", IEEE Transactions on Pattern Analysis and Machine Intelligence, Vol. 17, No. 2, pp.158-175
6. S. Loncaric, M. Subasic, E. Sorantin, "3-D deformable Model for Abdominal Aortic Aneurysm Segmentation from CT images",
7. T. McInerney and D. Terzopoulos, "Topologically Adaptable Snakes", Proc. of Fifth Int. Conf. on Compute Vision, Cambridge, 1995, pp. 840-845
8. K. Murase, S. Tanada, Y. Yasuhara, H. Mogami, A. Iio, K. Hamamoto, "SPECT volume measurement using an automatic threshold selection method combined with a V filter", Eur. J. Nucl. Med, 1989, Vol. 15, pp. 21-25.
9. S. Savolainen, H. Pohjonen, O. Sipilä and K. Liewendahl, "Segmentation method for volume determination with $^{111}\text{In}/^{99}\text{Tc}$ SPET", Nuclear Medicine Communications, 1995, Vol. 16, pp. 370-377